Journal of Engineering Physics and Thermophysics, Vol. 83, No. 1, 2010

INTERFERENCE AND DIFFRACTION OF PRESSURE SHOCKS IN FLOW AROUND BODIES OF REVOLUTION LOCATED NEAR A SURFACE

V. F. Volkov, E. K. Derunov, and A. I. Maksimov

UDC 519.85+533.696.5

This paper presents the results of experimental and computational investigations of a supersonic (M_∞ = 4.03, $Re_1 = 55\cdot10^6$ m^{-1}) flow around two bodies of revolution with conical noses with an opening $\theta = 40^o$ and cylindrical cases with an extension $\lambda = 5$ located near a flat surface at zero angles of attack at a relative distance from each other Z = 1.4. We have made a comparison between the structure of the shock waves formed in the zone of hydrodynamic interference of the bodies of revolution in free flight and in flight over the surface at a distance Y = 0.96. We have demonstrated the possibility of satisfactory prediction of the hydrodynamic structure of the realized flows and aerodynamic characteristics of the bodies under investigation on the basis of the numerical solution of Euler equations.

Keywords: *aerodynamic interference, experiment, body of revolution, plate, pressure shock, diffraction, pressure coefficient, Euler equations, wave structure.*

Introduction. The investigation of the supersonic flows realized in the flight of a group of vehicles near a surface is an urgent problem of modern aerogas dynamics. A detailed analysis of their gas-dynamic structure is necessary for explaining the effects of aerodynamic interference and predicting the appearance therewith of forces and moments. Since experimental studies of such complex flows are very difficult and require considerable expenses, an important role in solving problems of the considered class is played by the methods of computational aerodynamics. As is known, more complete modeling of the real properties of flows connected with viscous effects is only possible with the use of the methods of solving Navier–Stokes equations with different turbulence models (RANS) or direct numerical simulation (LES). These methods require huge computational resources and a considerable time expenditure. Therefore, in many cases, for practical purposes simpler and cheaper methods of obtaining necessary information on the basis of solving Euler equations are used. This was demonstrated, for example, in [1–9] in which a comparison between the results of numerical calculations of a nonviscous flow and the experimental data was made. The above-mentioned works showed a satisfactory agreement between the calculated and experimental aerodynamic characteristics of the investigated bodies, although in a number of cases considerable discrepancies in local pressure distributions were observed. Such differences are most often explained by the boundary-layer separations that take place in the real flow and are formed under the action of pressure shocks [8, 9].

The present work is a sequel of the investigations presented in [1–4, 6–8, 10–12]. The aim of the work is to consider in detail the wave structures formed in the process of interference-diffraction phenomena in the space between the bodies and the plate, as well as to check further the possibilities of using numerical calculations within the framework of Euler equations for investigating such complex flows.

Experimental. Experiments were carried out in a T-313 supersonic wind tunnel of the S. A. Khristianovich Institute of Theoretical and Applied Mechanics of the Siberian Branch of the Russian Academy of Sciences at a Mach number M_∞ = 4.03 and a Reynolds number $Re_1 \approx 55\cdot10^6$ m^{-1}. The model consisting of a flat plate FP and two identical bodies of revolution (B_1 and B_2) with an opening of their noses $\theta = 40^o$ located over it parallel to the flow is

S. A. Khristianovich Institute of Theoretical and Applied Mechanics, Siberian Branch of the Russian Academy of Sciences, 4/1 Institutskaya Str., Novosibirsk, 630090, Russia; email: volkov@itam.nsc.ru. Translated from Inzhenerno-Fizicheskii Zhurnal, Vol. 83, No. 1, pp. 98–110, January–February, 2010. Original article submitted November 12, 2008; revision submitted June 11, 2009.

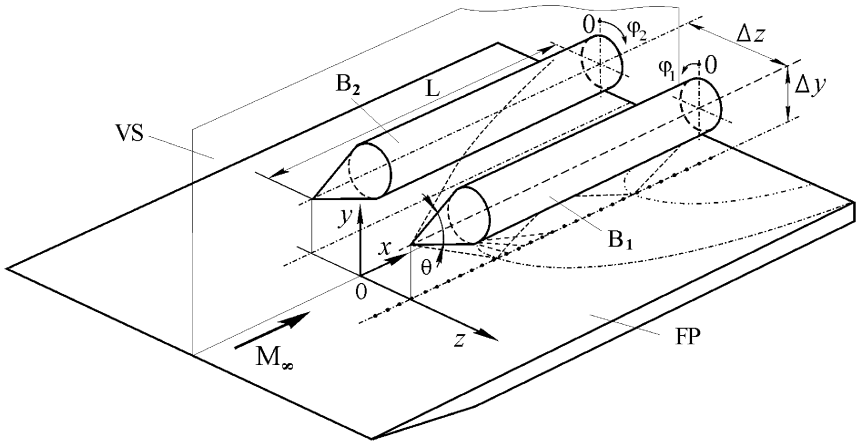

Fig. 1. Scheme of the model: B_1, main body of revolution; B_2, second body; FP, plate; VS, symmetry plane; θ, opening angle of the nose; φ_1 and φ_2, azimuth angles of the bodies of revolution.

schematically represented in Fig. 1. The extension of the cylindrical cases of the bodies $\lambda = (L - x_0)/D = 5$, where L and $x_0 = \dfrac{D}{2 \tan \dfrac{\theta}{2}}$ are the total length of the body and the length of the nose, respectively, and $D = 50$ mm is the case diameter. The relative distance of the axes of the bodies from the plate surface $Y = \Delta y/D$ was 0.96. In the case of the absence of the plate, optical visualization of the flow by an IAB-451 Toepler device was carried out with the bodies B_1 and B_2 located in one vertical plane. The relative distances Y between the bodies of revolution thereby were Z = 1.06–4.0 in the presence of the plate.

The distance x from the front edge of the plate to the joint of the cases of the bodies of revolution with their nose parts was equal to 110 mm. The thickness of the turbulent boundary layer on the plate in the vicinity of the incidence of the front shocks propagating from the bodies were within the limits $\delta \approx$ 1.8–2 mm. To measure the pressure distributions, on the body B_1 there were 85 drainage holes of diameter 0.5 mm each arranged along one longitudinal element with a variable spacing from Δx = 1.6 mm on the nose to 10 mm near the afterbody. Circular panoramas of the pressure distribution were obtained with the body B_1 rotating about its longitudinal axis with a fixed pitch $\Delta\varphi = 10^{\circ} \pm 0.3^{\circ}$. For analogous purposes, the plate was equipped with a special drained insert with 100 holes of diameter 0.5 mm each spaced at 3.5 mm in parallel to the x axis. The plate together with this insert was shifted by means of an electropneumatic device in the lateral direction with an analogous fixed spacing of 3.5 mm and permitted obtaining panoramas of the pressure distributions on an area with sizes up to 346.5 × 308 mm. The pressure was measured by means of an MID-100 multichannel device having in the 0–100-kPa range an error no higher than 0.3% of its upper limit.

Measurements of the longitudinal and normal forces **X** and **Y** and of the rolling moment $\mathbf{M}_x$ and the pitching moment $\mathbf{M}_z$ acting on the body B_1 were made by means of the issued four-component mechanical balance of the AV-313M wind tunnel, and the lateral force **Z** and the yawing moment $\mathbf{M}_y$ were registered by the two-component intramodel tensometric balance. According to the data of multiple measurements, the mean-square errors in determining the aerodynamic coefficients σ were: for C_y, 0.001; for C_z, 0.006; for m_y, 0.025; and for m_z, 0.021 (the forces thereby pertained to the free stream dynamic pressure q_∞ and the midsection of the body of revolution $S_m = \pi D^2/4$, and the moments pertained to $q_\infty S_m L$). The errors in determining the pressure coefficients C_P were estimated to be equal to ±0.014. To rectify errors connected with the nonuniformity of the flow in the working section of the wind tunnel, we subtracted from the pressure values realized on the body of revolution B_1 and on the plate the background pressure values that took place in an isolated flow around them, i.e., in the absence of the second body with the plate (in the first case) of of both bodies (in the second case). The patterns of the limiting streamlines on the surface of the plate and of the bodies of revolution were obtained by the method of oil-black visualization. A more detailed description of the structure of the models is given in [4].

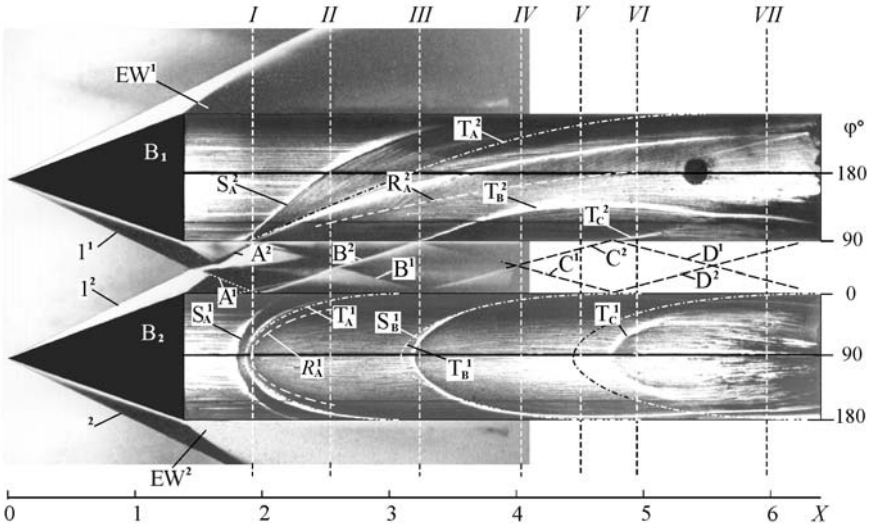

Fig. 2. Flow around bodies of revolution with $\theta = 40^{\circ}$ at $M_{\infty} = 4.03$ and $Z = 1.4$ (without a plate). EW, fan of expansion waves; *I–VII*, cross-sections.

Algorithm of Numerical Calculations. The numerical algorithm used for the calculations is based on Euler equations given in integral form [7]. The solution is sought in the Cartesian system of coordinates x, y, z in the domain bounded by the surface of the main body of revolution B_1, its front shock, and the symmetry plane between the bodies VS, and in the cases of the presence of the plate, also by the plate FP located under them (see Fig. 1). The solution domain is partitioned into finite nonoverlapping volumes. The gas-dynamic parameters on the cell faces of each elementary volume are determined by the linear interpolation of the corresponding values at nodal points.

A steady-state solution is obtained by setting in each section x = const and subsequent global iterations with the second order of accuracy for the space coordinates and with the first order of accuracy for the time. In so doing, the flow parameters in the first march section are calculated from the flow conicity condition in the vicinity of the nose of the body. In the process of obtaining a steady-state solution, correction of the position of the front shock wave is made. The boundary conditions are the conditions of no flow on the body and on the plate and of symmetry about the vertical plane VS. On the surface of the front shock wave, the flow parameters are defined by the Rankine–Hugoniot relations. The solutions obtained in the calculated domain are sewn together in the vertical half-plane ($\varphi = 180^{\circ}$) passing through the body axis. The computational algorithm is described in more detail in [7, 13].

For the problem under considerations, we used, as the initial data, the solution for an isolated body of revolution. Because of the limited resources of the personal computer used, calculations were carried out on a 190 × 100 × 150 mesh in the longitudinal (x), radial (r), and azimuthal (φ) directions, respectively, with separation of the front shock wave. In the r and φ directions, before the front shock waves met with the symmetry plane VS or with the plate, the mesh was uniform, while downstream, because of the adaptation to the outer boundaries, it became nonuniform in all directions. On the cylindrical part of the body of revolution, the mesh width nonuniformity reached $h_{\max}/h_{\min} = 3$.

Results of the Investigations. The supersonic flow around two bodies located close to one another and to a surface is characterized by their aerodynamic interference both with one another and with the plate. At angles $\theta \geq 40^{\circ}$ in the vicinity of incident front shock waves vast zones of spatial separation of the boundary layer are formed on the plate [11] and strongly influence the pressure distribution on it. Analogous phenomena are also observed on the surfaces of bodies of revolution.

Figure 2 is a picture of the flow around two bodies of revolution with openings of their noses $\theta = 40^{\circ}$ at a Mach number $M_{\infty} = 4.03$ and a relative distance between them $Z = 1.4$ in the case of the absence of the plate. To show the flow pattern more clearly, this picture is a combination of a shadow and an oil-black picture obtained in different experiments. It should be noted that on the second body of revolution B_2 the image of the limiting streamlines is displaced through 90°, i.e., its lateral surface facing the body B_1 is shown.

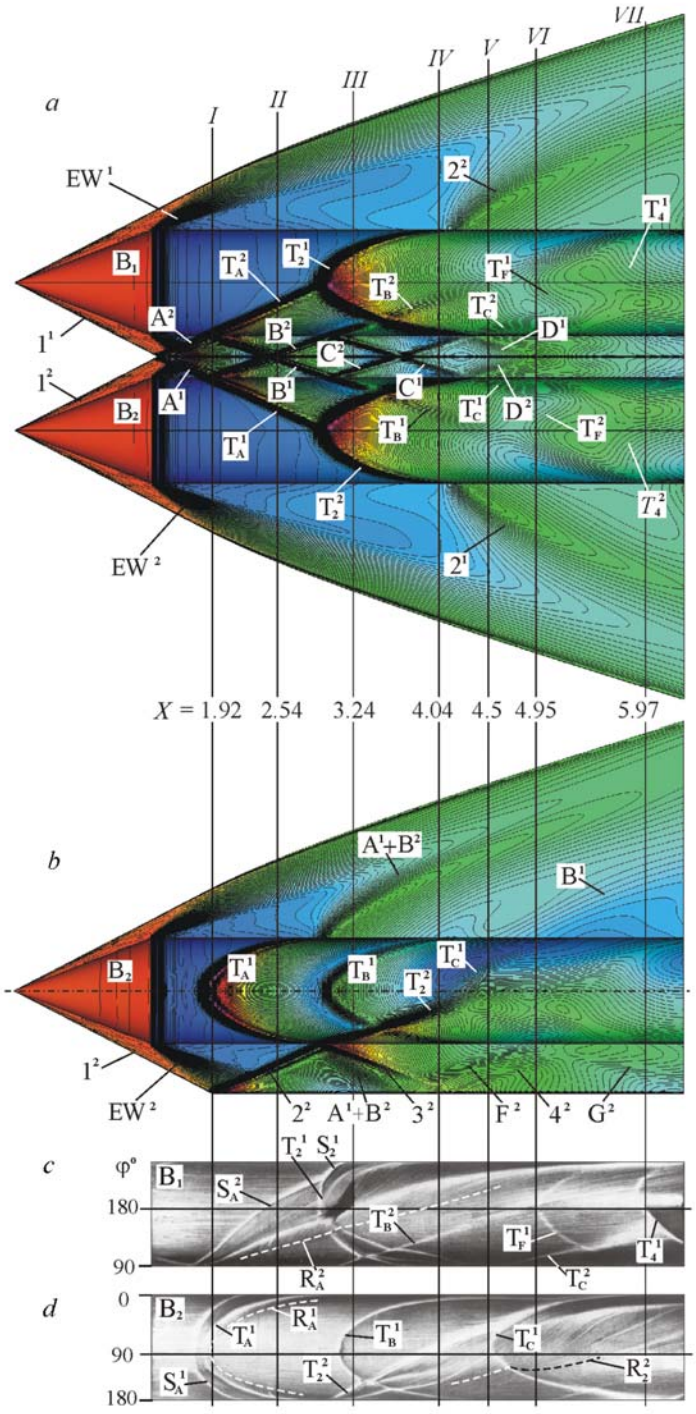

Fig. 3. Calculated density fields in the horizontal (a) and vertical (b) sections and limiting streamlines on the surface of the bodies of revolution (c, d) in the presence of a plate.

As is seen, the shock waves A formed after the front shock waves 1^1 and 1^2 meet with each other cause on the surfaces of the bodies large boundary-layer separations bounded by the lines of convergence of the limiting streamlines S_A^1, S_A^2 and their divergence R_A^1, R_A^2, respectively. The detached and closing shock waves formed therewith coalesce some distance from the bodies into single reflected shocks B^1 and B^2, which also lead to local boundary layer

separations in the vicinity of the point of their meeting with the surfaces of the bodies. Downstream the separation lines S_B gradually transform into the usual zones of convergence of the limiting streamlines, and the bright fringes observed below cross-section *IV* are simply passive drift lines of the oil-black mixture not connected with the action of the corresponding pressure shocks B^1 and B^2. The intensities of the repeatedly reflected shocks C^1 and C^2 are obviously no longer sufficient for the boundary-layer separation and can cause only local deviations of the limiting streamlines, forming traces T_C^1 and T_C^2.

The corresponding isodensity lines obtained in the calculations for the given case are in good agreement with the experimental data obtained. They only differ from the calculated flow patterns considered in [8] (for the case of $M_\infty = 4.03$, $\theta = 40^o$, $Z = 1.8$) by the forward shift of the lines of meetings of pressure shocks with the surfaces of the bodies and in the number of reflections of shock waves in the space between the bodies (four reflections instead of two), which is explained by the decrease in the Z value. As might be expected, the calculated traces T_A^1 and T_A^2 of shocks A^1 and A^2 depicted in Fig. 2 (dash-dot lines) are located practically midway between the experimental lines of convergence of the limiting streamlines S_A and their divergence R_A. However, the subsequent calculated traces of shocks B and C (see the lines T_B^1 and T_C^1 on the surface of the body B_2) are located somewhat higher than the traces formed in the experiment, and the divergence for the repeatedly reflected shocks C is much greater therewith.

Such a situation is also observed for the case of flow around the considered bodies in the presence of a plate. Figure 3 shows the calculated density fields in the horizontal section passing through the axes of the bodies of revolution when viewed from the side of the plate (a) and in the vertical plane intersecting the axis of the body B_2 (b), as well as the corresponding isolines (a, b) and the patterns of the limiting streamlines on the surfaces of the bodies of revolution obtained in the experiment (c, d). It should be noted here that before the zones where the pressure shocks 2 reflected from the plate reach the surfaces of the bodies, both the experimental (Fig. 2 and Fig. 3c, d) and calculated flow patterns are fully identical. In this case, the optical pictures of the flow around the models (except for the region between the bodies and the plate) are also practically identical. As is seen, the front shock waves 2^1 and 2^2 reflected from the plate lead to the appearance of arched higher-pressure zones (crowding together of isolines T_2^1, T_2^2) on the surfaces of the bodies which interact intensively with the higher-pressure zones T_A (Fig. 3a) and then with T_B and T_C formed under the action of the shock waves B and C reflected from the side surfaces (Fig. 3a, b).

The real flow pattern (Fig. 3c, d) is noticeably complicated due to the boundary-layer separations arising on the surfaces of the bodies under the action of the pressure shocks A and 2, as well as due to the interaction of the separation zones with one another. The shock waves A and 2 incident on the bodies have an intensity sufficient for the formation of not only main but also secondary flow separations situated between the S_A and R_A convergence lines, as well as between the analogous convergence S_2 and divergence R_2 lines. It can be noticed that because of the influence of the detached flow caused by the shock wave A, it is practically impossible to identify the R_2 line in the given pictures. The decrease in the intensity of shocks (density of isolines) in the process of their repeated reflections from the body surfaces and downstream propagation that appears in the calculations fully agrees with the gradual reduction of the traces of shocks and the disappearance of the signs of separation observed in the experiment. The significant decrease in the intensity of sequentially reflected shocks B, C, D (Fig. 3a) and 2, 3, 4 (Fig. 3b) is due to both their diffraction by the bodies of revolution and the action on them of expansion waves EW formed on the joint between the conical noses and the cylindrical cases and then reflected sequentially from the surfaces of the plate and the bodies of revolution.

As is seen from Fig. 3b, the pressure shock B^2 resulting from the reflection of the shock A^1 from the surface of the body B_2 (because of the insufficient resolution on the calculated isodensity curves they coalesce into combined curves designated as $A^1 + B^2$) is reflected from the plate surface in the form of the shock F^2 which forms on the surface of the body B_2 a weak trace T_F^2 (see Fig. 3a and its analog T_F^1 in Fig. 3c situated on the body B_1) and is reflected back in the form of the shock wave G^2. In turn shocks 3 are reflected from the plate in the form of shocks 4 propagating towards the bodies following shocks F at a marked distance form them. In the real flow, shocks 4 reach the bodies near their rear ends and leave arched traces T_4 on their downstream faces (see Fig. 3c). In the calculated patterns (Fig. 3a) their traces appear only in the form of a wide band of weak, close isodensity curves having no appreciable effect on the pressure distribution. The processes of interference and diffraction of all these shocks of complex configuration will become more clear upon considering the spatial structure of the considered flow and cross-sections *I–VIII* in moving down the stream described below.

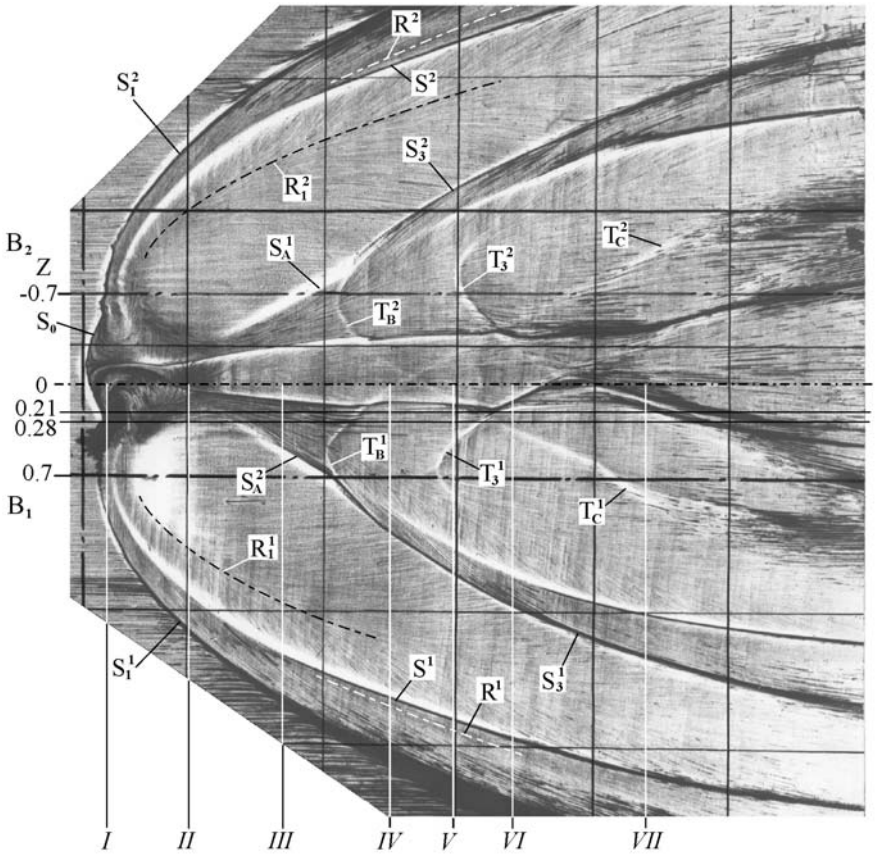

Fig. 4. Oil-black pattern of the limiting streamlines on the plate surface at $M_\infty = 4.03$, $\theta = 40^o$, and $Z = 1.4$.

The simultaneous interaction of the front, reflected, and diffracting pressure shocks leads to the formation of a rather complex flow pattern (Fig. 4) on the FP plate as well (Fig. 1). Front shock waves 1 cause, on the plate surface, developed boundary-layer separations along the convergence curves S_1^1 and S_1^2, as well as secondary separations bounded by the curves S^1, R^1, and S^2, R^2, respectively. Additional separations connected with the curves S_A^1 and S_A^2 arise under the influence of shocks A diffracting by the bodies. When the convergence curves S_A^1 and S_A^2 meet with traces T_B^2 and T_B^1 (approximately midway between cross-sections *III* and *IV*), the simultaneous action of shocks A and B leads to the formation of additional zones of developed separation along the curves S_3^1 and S_3^2. The repeatedly reflected shocks 3 having a low intensity are able to form only rather weak traces of local deflections of the limiting streamlines T_3^2 and T_3^1, respectively. A more thorough analysis permits revealing also the influence of very weak shocks C leading to the appearance of traces T_C which noticeably bend the propagation direction of traces T_B before cross-section *VII*.

Unfortunately, because of the uncontrollable differences in deformations of the holders used to fasten the bodies of revolution, it was impossible in the considered experiment to provide full symmetry of the flow about the vertical symmetry plane VS (lines $Z = 0$ in Fig. 4). For example, the traces of pressure shocks T_B^2, T_3^1, and T_C^2 on the plate are markedly shifted downstream from the corresponding traces T_B^1, T_3^1, and T_C^1 located under the body of revolution B_1. However, such asymmetry does not lead to a strong distortion of the general flow pattern and practically does not hinder not only a qualitative but also a quantitative comparison between calculated and experimental data.

The shadowgraph (see Fig. 2) shows that in the flow around the bodies without a plate at $M_\infty = 4.03$, $\theta = 40^o$, and $Z = 1.4$ front shocks 1 and reflected shocks B and C interact with each other regularly. At the same time in the presence of a plate ($Y = 0.96$) the pattern of oil-black visualization of the limiting streamlines (Fig. 4) points to the Mach interference of detached shocks resulting from the interaction of front shocks with the boundary layer. Such interaction of shocks near the plate surface leads to the appearance of a convex curve of the developed separation S_0

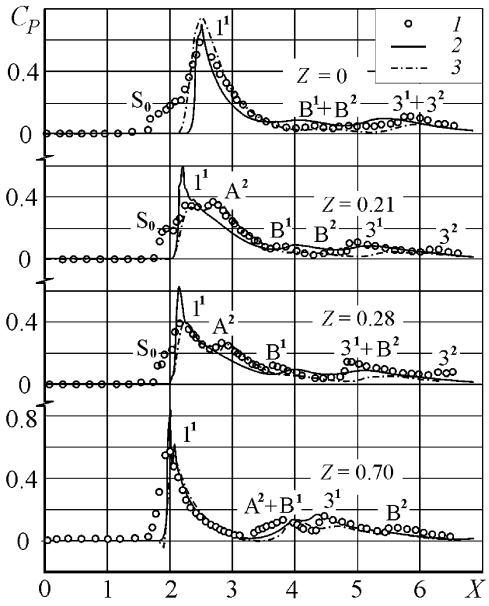

Fig. 5. Distribution of pressure coefficients on the plate surface.

connecting curves S_1^1 and S_1^2. The topological features of the flow realized on the plate surface in the flow around bodies with different angles θ separated by a relative distance in the range of Z = 1.06–3 were considered in detail in [11, 12].

Direct comparisons of the distributions of pressure coefficients C_P in four arbitrarily chosen longitudinal sections on the plate surface (Fig. 5) demonstrate a plausible agreement between the experimental (1) and calculated (2, 3) data. Here curves 2 present the results of the calculations performed, and curves 3 were taken from [4] where they were also obtained in numerical modeling with the use of Euler equations.

In all longitudinal sections situated between the vertical symmetry plane and the projection of the axial line of the body B_1 (see Fig. 4), except for the zones where the pressure begins to increase, both calculations are close to the experiment. The discrepancies in the initial area of pressure increase are due to the boundary-layer separation taking place in the real flow, which cannot be modeled within the framework of calculations in the nonviscous approximation. The maximum discrepancy between the positions of the experimental and calculated points of onset of pressure increase takes place in the section Z = 0, which is due to the formation of a large zone of reverse flow with a bulging-out line S_0 of the boundary-layer separation (Fig. 4).

It should be noted that in the region of the first (main) pressure peaks formed under the action of the front shock 1 calculations 3 demonstrate a better agreement with the experiment than calculations 2. The appreciably higher peak pressure values on curves 2 are primarily due to the strong mesh irregularity that took place in the region where the front shocks met with the plate surface. The lower-lying local pressure increases arise under the action of the corresponding pressure shocks indicated over the distribution plots of pressure coefficients.

The development of the spatial structure of the flow moving downstream in the process of interference and diffraction of pressure shocks in the absence and presence of a plate is illustrated in Figs. 6 and 7, which show the calculated pressure fields and isodensity curves in the chosen cross-sections. Since the flow around the bodies without a plate is characterized by full symmetry of the flow about both the vertical plane VS and the horizontal plane HS passing through the axes of the bodies, the complete flow patterns are given, as an example, only for cross-sections *I* and *II* (Fig. 6a and b).

It should be noted that because of the insufficient density of the chosen mesh (190 × 100 × 150) and the low order of accuracy of the computational algorithm used, in moving downstream the crowds of isodensity curves corresponding to the pressure shocks blur rather rapidly. Therefore, to make the configurations of the considered shocks more distinct, Fig. 6d, f and h for cross-sections *III–V* and Fig. 7d and f for cross-sections *IV*, *V* show additionally the schemes of the corresponding wave structures.

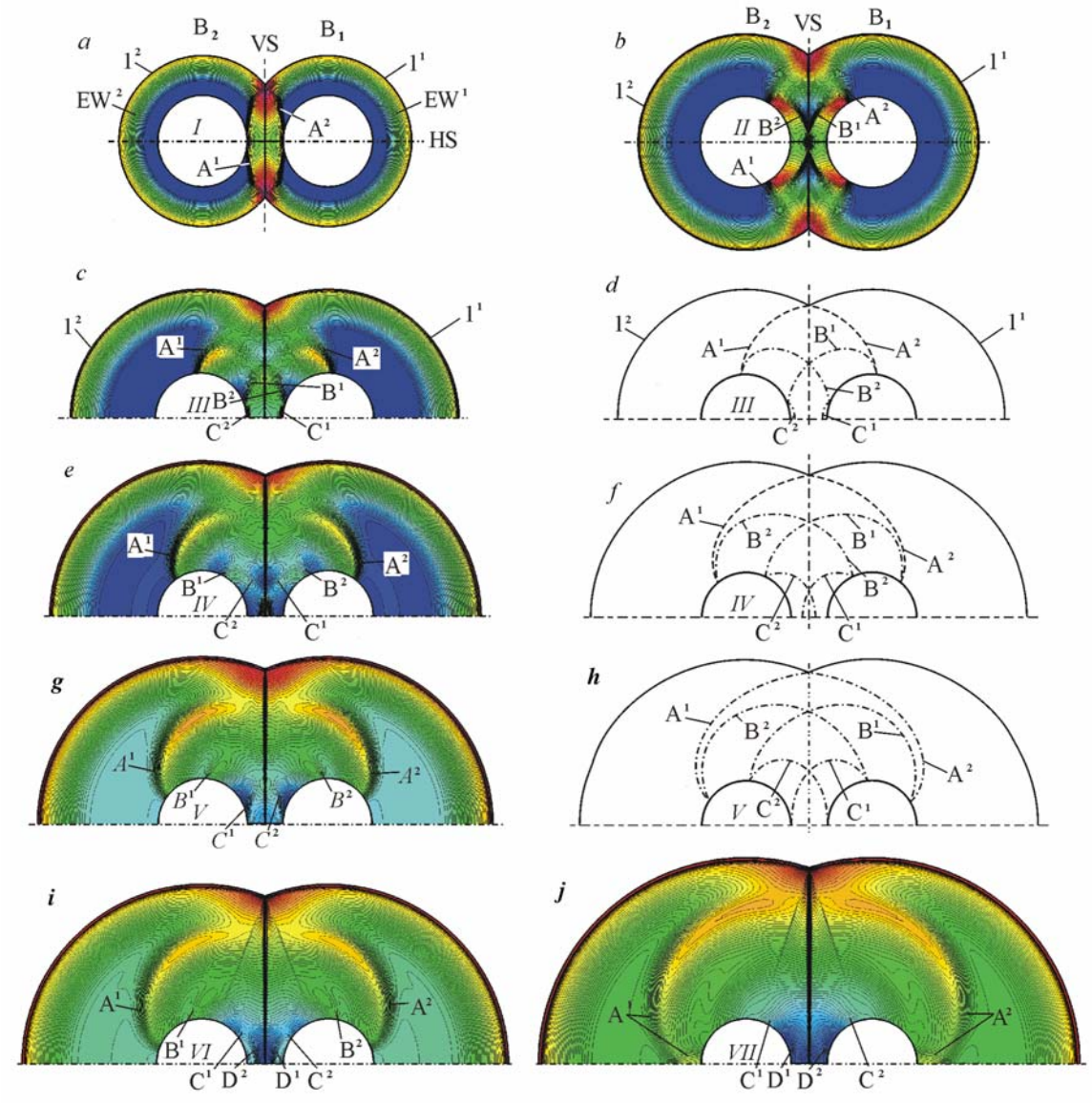

Fig. 6. Calculated density fields in cross-sections *I–VII* (X = 1.92, 2.54, 3.24, 4.04, 4.50, 4.95, and 5.97) realized in the case of the flow around two bodies of revolution with $\theta = 40^{o}$ at $M_{\infty} = 4.03$ and Z = 1.4.

As is seen from Fig. 6a, in cross-section *I* (X = 1.92) the pressure shocks A^1 and A^2 resulting from the interaction of the front shocks 1^1 and 1^2 (see Fig. 2) reach the lateral surfaces of the bodies of revolution, after which the simultaneous process of their back reflection and diffraction by the bodies begins. Simultaneously with this in the space between the shocks A^1 and A^2 interference of the fans of expansion waves EW^1 and EW^2 formed at the joint between the noses and the cases of the bodies of revolution (see Figs. 2 and 3a, b) takes place. Downstream, in cross-section *II* (X = 2.54) the reflected shock waves B^1 and B^2 cross the vertical symmetry plane VS (Fig. 6b), and in cross-section *III* (X = 3.24) repeatedly reflected shock waves C^1 and C^2 arise (Fig. 6c, d). When these bodies are separated by a distance Z = 1.8, the analogous stages of interference and diffraction of shocks are observed much later, only at X = 2.76, 4.2, and ~5.5 respectively [8], which points to a noticeable complication of the flow pattern with decreasing distance between the bodies.

With further downstream displacement (Fig. 6e–h) shocks C^1 and C^2 reach the lateral surfaces of the neighboring bodies and are reflected in the form of shocks D (Fig. 6i). At the same time the process of diffraction of the shocks A and B by the bodies of revolution goes on. Before cross-section *VII* the upper and lower branches of the

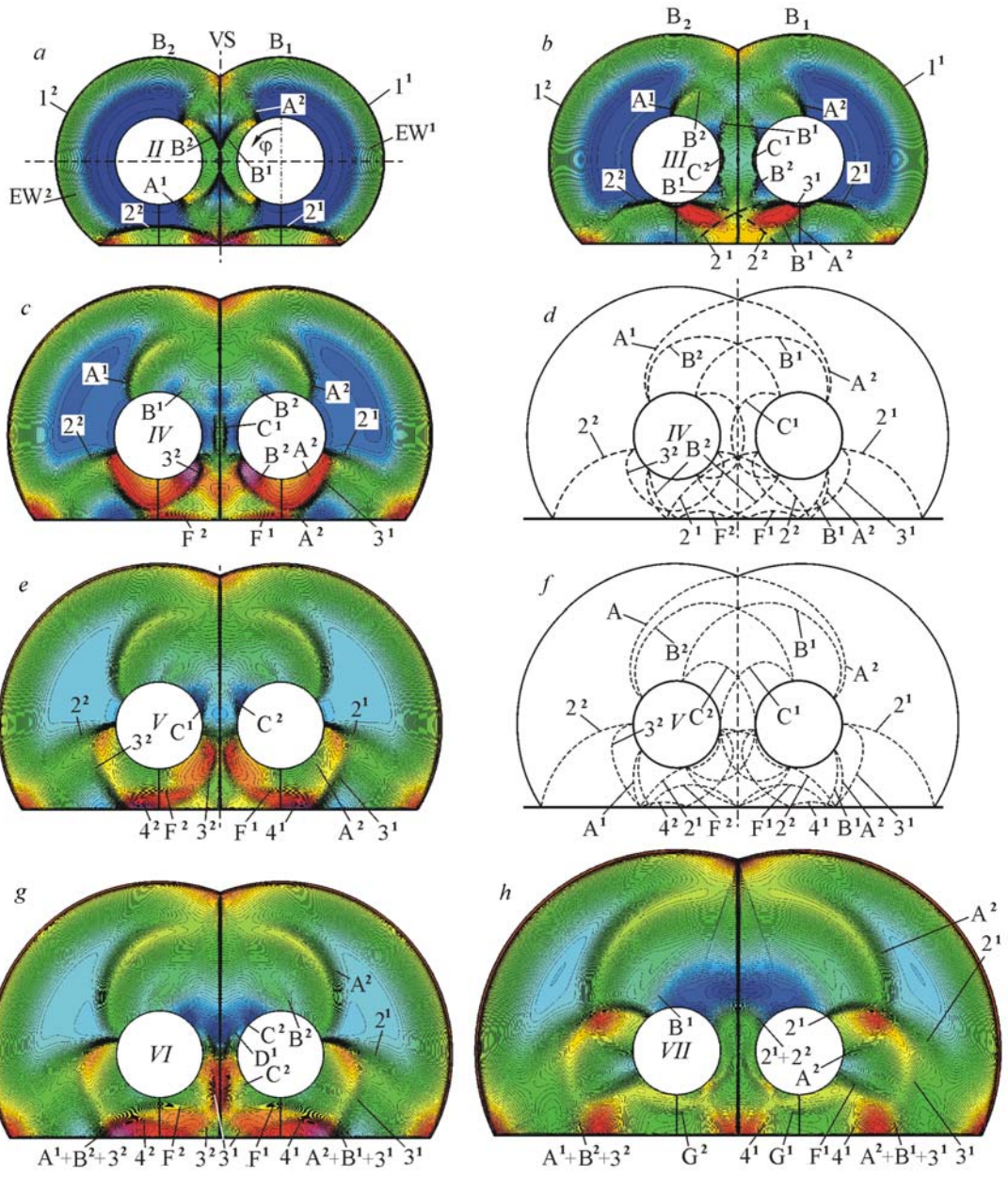

Fig. 7. Calculated density fields in cross-sections *II*–*VII* in the flow around two bodies of revolution with $\theta = 40^{o}$ at $M_{\infty} = 4.03$ and $Z = 1.4$ in the presence of a plate ($Y = 0.96$).

shocks A^1 and A^2 meet with each other and intersect the horizontal symmetry plane of the flow from outside the bodies of revolution and continue to propagate farther (Fig. 6j). Following the shocks A^1 and A^2, with a delay by azimuth angles $\varphi \approx 50$–60^{o}, the reflected shocks B^1, B^2, and C^1, C^2 also diffract (Fig. 6c–i).

The flow around the bodies in the presence of a plate (Fig. 7) is characterized by a significant complication of the pattern of interaction between the pressure shocks mainly in the space between the bodies and the plate. While in the upper part of the flow (before the horizontal plane passing through the axes of the bodies) up to cross-section *V* (Fig. 6a–h and Fig. 7a–f) the patterns of the fields and isodensity curves remain completely identical, in the space between the bodies and the plane already in cross-section *II* (Fig. 7a) interference of shocks A^1 and A^2 with shock waves 2^2 and 2^1 reflected from the plate is observed. Downstream all the other pressure shocks resulting from sequential reflections from the plate and the surfaces of the bodies of revolution, as well as the fans of expansion waves

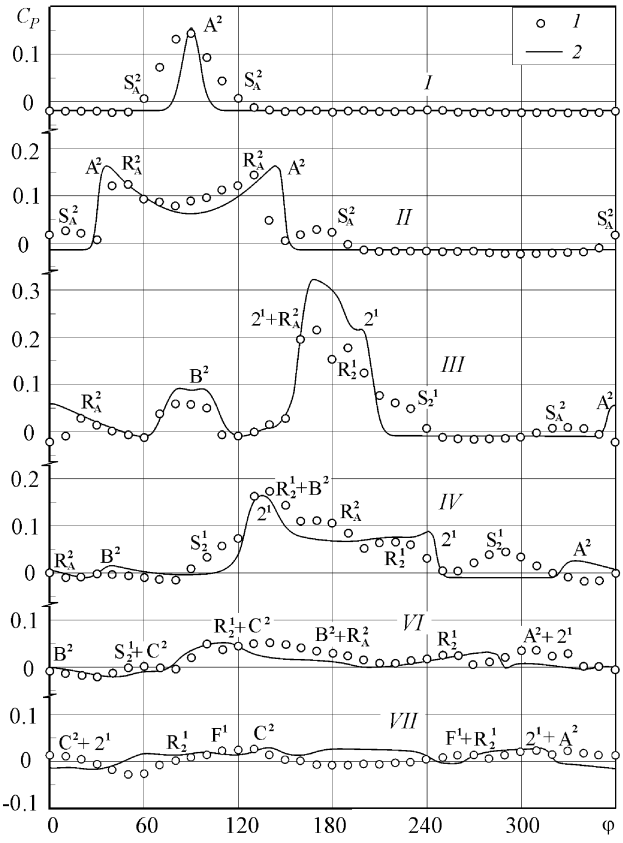

Fig. 8. Distribution of pressure coefficients on the surface of the bodies of revolution in cross-sections X = 1.92, 2.54, 3.24, 4.04, 4.95, and 5.97 at $\theta = 40^{o}$, M_{∞} = 4.03, and Z = 1.4 in the presence of a plate: 1) experiment, 2) calculation.

EW^1 and EW^2 (Fig. 7b–h), become gradually involved in the interference and diffraction processes. Figures 7b–7d confirm that the shocks dissected by the vertical plane and designated in Fig. 3b as $A^1 + B^2$ in fact represent two closely spaced diffracted (A^1) and reflected (B^2) pressure shocks which had no time to move apart for a distance sufficient for their identification on the isodensity curves in the form of individual shocks. Likewise, Figs. 7c–7f show that shocks F^1 and F^2 are formed due to the reflection of the lower branches of the shocks B^1 and B^2 from the plate. It may be noted thereby that the reflected shocks F^1 and F^2 are in fact markedly displaced from the projections of the longitudinal axes of the bodies of revolution on the plate towards the vertical symmetry plane VS, which completely agrees with the experimental data (see the traces of shocks T_B^1 and T_B^2 in Fig. 4). Likewise, the isodensity curves obtained in the calculations make it possible to follow the appearance and development of shocks 4 reflected from the plate (Fig. 7e–h) which, vice versa, are somewhat shifted towards the outside from the projections of the axes, which is also in good agreement with the experiment (see the trace T_3^2 in Fig. 4). The slight shift of the trace T_3^1 in the experiment towards the second body of revolution is explained by the above-mentioned small asymmetry of the flow about the mean line 0 (the line of intersection of the plane VS with the plate).

Comparison between the experimental and calculated data shows their complete agreement except for the effects connected with boundary-layer separations on the plate and the bodies of revolution. Figure 8 demonstrates graphically the degree of significance of their influence on the local pressure distributions on the body of revolution. In the cross-sections *I–IV* obtained in the experiment and in the calculation, there is a fairly good agreement between the main higher-pressure zones formed under the action of shocks A^2, 2^1, and B^2 on the surface of the body B_1, but the boundary-layer separation in the real flow leads to an earlier increase in the pressure in the region of the separation lines S_A^2. It should be noted thereby that the regions where $C_P < 0$ are zones of influence of the fans of expansion waves EW issuing from the joint between the noses and the chassis of the bodies of revolution, which are observed very well in the corresponding density fields (see Fig. 6a and Fig. 7a–c). In moving

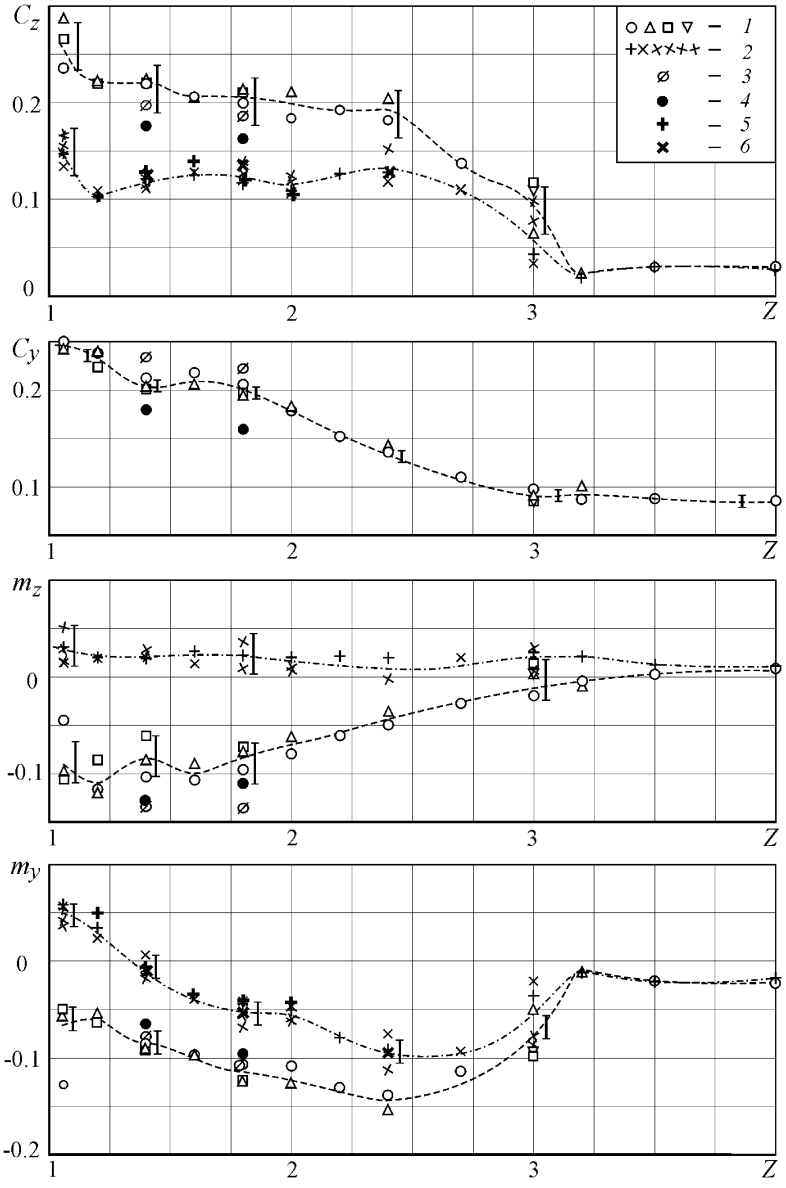

Fig. 9. Aerodynamic characteristics of the body of revolution B_1 at $M_\infty = 4.03$ and $\theta = 40^o$.

downstream, the higher-pressure zones S_A^2 and S_A^1 caused by detached shocks extend in the azimuthal direction and lead to appreciable differences from the calculated data. For example, already in cross-section *II* ($X = 2.54$) the difference in angular coordinates of the points of onset of pressure increase in the experiment and in the calculation reaches ~40–50°, and further downstream it becomes even greater and in cross-sections *VI* and *VII* only qualitative similarity between the data obtained is observed.

It should be noted that both the experiment and the calculation in cross-section *III* clearly register a considerable increase in the pressure in the sector of $\varphi \approx 160$–210^o caused by the simultaneous action of intensive shocks A^2 and 2^1 (see Fig. 3c and Fig. 7b). It should also be noted that the discrepancies between the calculated and experimental pressure distributions near the afterbody, by virtue of their small values, practically have no effect on the total aerodynamic characteristics of the bodies of revolution, as evidenced by the data of Fig. 9.

Figure 9 shows the aerodynamic characteristics of the body of revolution B_1 obtained at $M_\infty = 4.03$ and $\theta = 40^o$ in the variation range of the distance between the bodies $Z = 1.06$–4. On the graphs, points 1 and 2 pertain to measurements using an AV-313M mechanical balance for flow around the bodies in the presence and absence of a

plate, respectively (individual marks belong to different sets of repeated tests), points 3 pertain to the data obtained by integrating the pressure distributions on the surface of the body B_1, points 4 and 5 pertain to the calculations performed in the present work for flow around two bodies in the presence of a plate and without it respectively, and points 6 pertain to the calculation made in [4]. Vertical segments of the lines show balance measurement errors equal to $\pm 3\sigma$. The auxiliary dashed and dashed-dot lines serve only for connecting the approximately averaged results of multiple balance tests.

Comparison of the results presented in Fig. 9 points to a good agreement between the experimental and calculated data whose deviations in most cases do not exceed values of $\pm 3\sigma$, i.e., the accuracy of balance tests. The exception is only the evidently fallen-out experimental points (circles on the graphs m_z and m_y at $Z = 1.06$ and some marks at $Z = 3$) and the calculated values of the normal force coefficients C_y, although the general tendency for deviation of calculated data towards underestimated values catches attention. For the cases of flow around bodies of revolution without a plate, both calculations demonstrate a good agreement both with the experiment and with each other.

As is seen from the data presented, over the entire investigated range of Z the coefficients of the lateral force C_z and normal force C_y are positive, i.e., the bodies are subjected to pushing-apart forces smoothly decreasing with increasing distance between the bodies. The coefficients of pitching m_z and yawing m_y moments calculated for the nose of the body of revolution indicate that in the presence of the plate the normal force **Y** causes a pitchup ($m_z < 0$), and the lateral force **Z** tends to turn the nose parts of the bodies laterally from each other ($m_y < 0$).

Conclusions. The simultaneous analysis of the experimental and calculated data has made it possible to follow the details of the development of the interference-diffraction phenomena arising in the supersonic flow around two bodies of revolution in the presence and in the absence of a flat surface located at a relative distance $Y = 0.96$. The possibilities of using numerical calculations on the basis of Euler equations for predicting the properties of such complex flows have been demonstrated, and a satisfactory agreement between the experimental and calculated data for both the position of the pressure shocks formed in the process of their interference and diffraction and the pressure distributions on the plate and on the bodies of revolution has been revealed. It has been shown that simultaneous use of experimental and calculated data (even those obtained in the nonviscous approximation) considerably facilitates the analysis of the spatial structure of the realized flows. For further improvement of the calculations of the considered flows on the basis of Euler equations, it is necessary to sue finer meshes and computational algorithms of a higher order of accuracy, and for their more complete modeling it is desirable to perform calculations on the basis of Reynolds-averaged Navier–Stokes equations with the use of rational turbulence models.

NOTATION

$C_P = (P - P_\infty)/q_\infty$, pressure coefficient; C_y, C_z, coefficients of lifting (normal) and lateral (pushing-apart) forces; D, case diameter, mm; h, computational mesh width on the x axis; L, total length of the body of revolution, mm; $\mathbf{M}_x$, $\mathbf{M}_y$, $\mathbf{M}_z$, aerodynamic rolling, yawing, and pitching moments; M_∞, Mach number of the undisturbed flow; m_y, m_z, coefficients of yawing and pitching moments; P, static pressure, N/m^2; $q_\infty = \rho V^2/2$, free stream dynamic pressure, N·m/sec^2; r, radial coordinate of the mesh space; R, divergence curve of limiting streamlines (flow attachment); Re_1, Reynolds number for the characteristic size of 1 m; S_m, midsection of the body of revolution; x, y, z, axes of the Cartesian coordinate system; $X = \Delta x/D$, $Y = \Delta y/D$, and $Z = \Delta z/D$, relative distances from the noses of the bodies of revolution, from their longitudinal axes to the plate surface, and between their axes, respectively; **X**, **Y**, **Z**, longitudinal, normal, and lateral (transverse) aerodynamic forces; δ, boundary layer thickness, mm; φ, azimuth angle, deg; λ, extension of the cylindrical case; θ, opening angle of the noses of the bodies of revolution, deg; σ, standard deviation of the normal distribution. Subscripts: ∞, undisturbed flow; max and min, maximum and minimum values of the parameter; m, midsection.

REFERENCES

1. A. V. Zabrodin, A. E. Lutskii, M. D. Brodetskii, and E. K. Derunov, Comparison between the results of computational and experimental investigations of the supersonic flow around a combination of two bodies of revolution, *Teplofiz. Aéromekh.*, **2**, No. 2, 97–102 (1995).

2. V. F. Volkov, Development of numerical methods on the basis of Euler equations as applied to supersonic aerodynamics problems, *Proc. Int. Conf. on the Methods of Aerophysics Research*, Pt. 1, Novosibirsk (1998), pp. 228–233.
3. M. D. Brodetskii, E. K. Derunov, A. M. Kharitonov, A. V. Zabrodin, and A. E. Lutskii, Interference of bodies in a supersonic flow. 1. Flow around one body of revolution over a plane surface, *Teplofiz. Aéromekh.*, **5**, No. 3, 301–306 (1998).
4. M. D. Brodetskii, E. K. Derunov, A. M. Kharitonov, A. V. Zabrodin, and A. E. Lutskii, Interference of a combination of bodies in a supersonic flow. 2. Flow around two bodies of revolution over a plane surface, *Teplofiz. Aéromekh.*, **6**, No. 2, 165–172 (1999).
5. V. V. Eremin, V. A. Mikhalin, and A. V. Rodionov, Calculation of the aerodynamic interference of the elements of carrier rockets at supersonic velocities, *Aéromekh. Gaz. Dina*m., No. 1, 24–35 (2002).
6. V. F. Volkov, E. K. Derunov, A. A. Zheltovodov, and A. I. Maksimov, Verification of numerical computations of supersonic flow around two bodies of revolution in the presence of a surface, *Proc. Int. Conf. on the Methods of Aerophysics Research*, Pt. 1. Novosibirsk (2004), pp. 214–221.
7. V. F. Volkov and E. K. Derunov, Mathematical modeling of the interaction of shock waves in the supersonic flight of a group of bodies, *Vychisl. Metody Programmir.*, **6**, No. 1, 75–85 (2005).
8. V. F. Volkov and E. K. Derunov, Interaction of a combination of bodies in a supersonic flow. Interference and diffraction of shock waves in the flow around two bodies of revolution, *Inzh.-Fiz. Zh.*, **79**, No. 4, 81–90 (2006).
9. V. V. Kovalenko and A. N. Kravtsov, Aerodynamic interaction of several bodies at supersonic velocities, *Uch. Zap. TsAGI*, **29**, Nos. 1–2, 31–38 (2008).
10. E. K. Derunov, A. A. Zheltovodov, and A. I. Maksimov, Peculiarities of 3-D flow development at impinged and swept shock wave/surface interactions, *Proc. Int. Conf. on the Methods of Aerophysics Research*, Pt. 1, Novosibirsk (2002), pp. 67–73.
11. E. K. Derunov, A. A. Zheltovodov, and A. I. Maksimov, Development of three-dimensional turbulent separation in the vicinity of incident intersecting compression shocks, *Teplofiz. Aéromekh.*, **15**, No. 1, 31–58 (2008).
12. E. K. Derunov, V. F. Volkov, A. A. Zheltovodov, and A. I. Maksimov, Analysis of the supersonic flow around two bodies of revolution near a surface, *Teplofiz. Aéromekh.*, **16**, No. 1, 13–36 (2009).
13. V. F. Volkov, *Algorithm of a numerical solution of the problem of three-dimensional supersonic interaction of two bodies* [in Russian], Preprint No. 29–87 of the Institute of Theoretical and Applied Mechanics, Siberian Branch of the USSR Academy of Sciences, Novosibirsk (1987).